Growth of Pagoda-Topped Tetragonal Copper Nanopillar Arrays

I-Chun Chang,[†,‡] Ting-Kai Huang,[†] Huang-Kai Lin,[†] Yu-Feng Tzeng,[†] Chih-Wei Peng,[†] Fu-Ming Pan,[‡] Chi-Young Lee,[§] and Hsin-Tien Chiu*[,†]

Departments of Applied Chemistry and of Materials Science and Engineering, National Chiao Tung University, Hsinchu, Taiwan 30050, Republic of China, and Center for Nanotechnology and Materials Science, National Tsing Hua University, Hsinchu, Taiwan 30043, Republic of China

ABSTRACT Growth of arrays of pagoda-topped tetragonal Cu nanopillar (length $1-6\,\mu$m; width 150 ± 25 nm) with {100} side faces on Au/glass is achieved by a simple electrochemical reduction of $CuCl_2$(aq) by Al(s) in aqueous dodecyltrimethylammonium chloride. Field-emission measurement shows that the Cu nanopillars can emit electrons ($10\,\mu A\,cm^{-2}$) at a turn-on field of $12.4\,V\,\mu m^{-1}$ with a calculated field enhancement factor of 713.

KEYWORDS: electrochemical reduction • pagoda • copper • nanopillar • field emission

One-dimensional (1D) metal nanowires (NWs), nanorods (NRs), and nanobelts have attracted considerable attention because of their promising future applications (1−17). However, facile and controllable fabrication of free-standing metal NW arrays is still a difficult challenge. Hard templates with 1D channels, such as anodic aluminum oxide and iontracked membranes, were often employed for high-density 1D metal growth (8−13). Hard-template-free processes are rare. Recently, pentatwinned Cu NWs grown upward on hard substrates by chemical vapor deposition (CVD) were reported (14, 15). Nevertheless, CVD is complicated and usually requires elaborate processing equipment. Recently, we have demonstrated that, by using simple galvanic displacement reactions, novel nanostructures of Cu, Ag, and Au can be grown efficiently on conducting substrates (18, 19). In these cases, the morphology of the products was adjusted by suitable surfactants, acting as growth control agents. Here, we report the growth and characterization of an unusual new type of 1D pagoda-topped tetragonal Cu nanopillar arrays, previously unknown in the literature, by this route. In addition, our preliminary investigation demonstrates that the Cu nanopillars can emit electrons efficiently under applied electrical fields.

Onto a glass substrate coated with Au (Au/glass) was pasted a slice of Al metal foil. Then the substrate was immersed in an aqueous solution containing $CuCl_2$ and dodecyltrimethylammonium chloride (DTAC) at 290 K. The Au surface turned black and then dark red as the reaction proceeded. After 7 h, the product was removed from the reaction medium for characterizations. An X-ray diffraction (XRD) study of the product showed a reflection pattern consistent with that of face-centered-cubic (fcc) Cu (JCPDF 89-2838; see Figure S1 in the Supporting Information). Figure 1a shows a field-emission scanning electron microscopic (SEM) image of the product on the substrate. The image displays densely grown straight 1D NRs pointing randomly. An energy-dispersive spectrum (EDS; inset Figure 1a) confirms that the NRs are composed of Cu mainly. The Pt signal is due to a sputtered Pt thin layer for clear SEM observation. The C signal may originate from the surfactant while the tiny O signal is a consequence of the surface oxidation of Cu during the sample preparation under atmospheric conditions. Figure 1b shows a side view of the

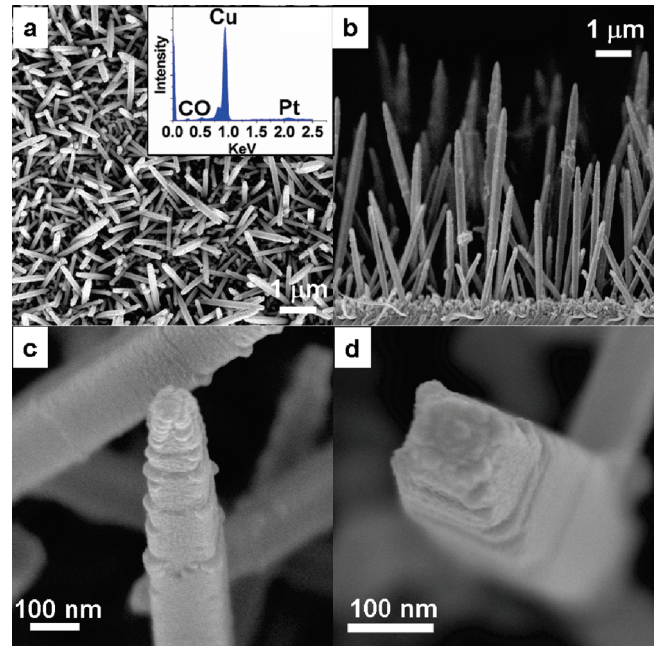

FIGURE 1. SEM images of Cu nanopillars on Au/glass: (a) top view (inset: EDS); (b) side view; (c) side view and (d) top view of a pagoda-shaped tip.

* Corresponding author. Phone: 886-3-5131514. Fax: 886-3-5723764. E-mail: htchiu@faculty.nctu.edu.tw.
Received for review April 20, 2009 and accepted June 24, 2009
[†] Department of Applied Chemistry, National Chiao Tung University.
[‡] Department of Materials Science and Engineering, National Chiao Tung University.
[§] National Tsing Hua University.
DOI: 10.1021/am900264u

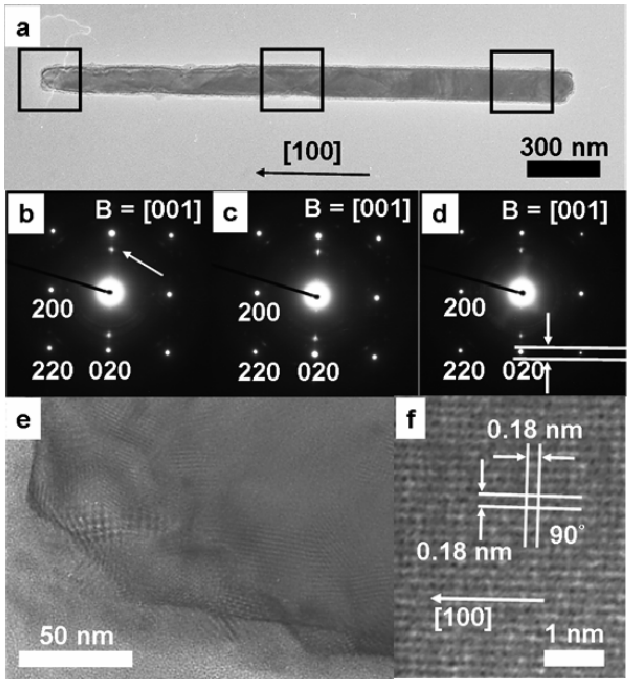

FIGURE 2. TEM studies of a Cu nanopillar: (a) low-magnification image; (b−d) SAED patterns of the rectangular marks in part a indicating the tip, middle, and bottom of the nanopillar (from left to right), respectively; (e) enlarged image of the lower half of the tip in part a; (f) HR image of the tip in part a.

product on Au/glass. This exhibits an array of NRs aiming upward. The NRs are 1−6 μm long and 150 ± 25 nm wide. Some of the longest NRs show length-to-width aspect ratios close to 50. Between the array and substrate, there is a layer (0.6 μm in thickness) of nanoparticles (NPs; 30−50 nm in size), presumably formed at the early growth stage. Parts c and d of Figure 1 show enlarged views of a typical NR tip found in the array, revealing its four-side pagoda-like morphology. The pagoda has a height of 400 nm and a bottom perimeter of 600 nm. The images also suggest that the NR's main body has an apparent tetragonal geometry. This is confirmed by the observation of an idealized tetragonal-shaped NR with a flat top square face in an SEM image (Figure S2 in the Supporting Information). Thus, we conclude that the majority of the NRs has a tetragonal pillarlike main body with a pagoda-shaped tip. Consequently, we name this unique type of new structure a "pagoda-topped tetragonal Cu nanopillar". Arrays of nanopillars can be grown only under specific sets of reaction conditions. The same results were obtained when identical reaction conditions were employed. Varying these generated other morphologies, ranging from NPs to pine-tree-like dendrites (Figures S3−S6 in the Supporting Information). A growth pathway will be proposed below based on the observations.

Figure 2a shows a low-magnification transmission electron microscopic (TEM) image of a representative nanopillar with an overall length of 3.6 μm. Regions selected from the tip, the body, and the root of the nanopillar, as shown in Figure 2a, have side widths of 100, 130, and 130 nm, respectively. Their corresponding selected-area electron diffraction (SAED) patterns are displayed in Figure 2b−d, respectively. All three images present identical square-shaped spot patterns, revealing the single-crystalline nature of the nanopillar. The d spacing estimated from the spots closest to the beam center is 0.18 nm. This is consistent with the d spacing of Cu(200) planes (JCPDF 89-2838). Thus, the lattice parameter a is determined to be 0.36 nm, consistent with the reported value of fcc Cu. From the patterns, the crystallographic zone axis can correspond to [001]. In addition to the spots of Cu, there are extra dim spots, as shown by the one indicated by an arrow in Figure 2b. These suggest the presence of a tiny quantity of Cu_2O. From this set of spots, a d spacing of 0.25 nm is estimated and assigned to be the d spacing of $Cu_2O(111)$ planes, 0.246 nm (JCPDF 78-2076). Figure 2e shows an enlarged image of the lower half of the tip shown in Figure 2a. Complex contrasts are observed in the image. This may be the result of uneven side walls of the pagoda-shaped structure, as indicated in Figure 1c,d. Besides, complicated Moiré fringes also exist in Figure 2e. Figure 2f shows a high-resolution TEM (HRTEM) image of the tip. In contrast to the HRTEM image from other portions of the nanopillar (Figure S7 in the Supporting Information), the fringes observed in this area are less straight and more blurry. Nonetheless, areas composed of aligned fringes can still be observed. These fringes are spaced 0.180 nm apart, consistent with the d spacing of Cu{200} planes (JCPDF 89-2838). The dihedral angle of 90° is also consistent with the theoretical value of Cu. Using the information discussed, the growth direction of the nanopillars is determined to be along the [100] direction, while the four side walls are bounded by the {100} planes. Apparently, many defects may exist in the region. To clarify this, we carried out Fourier transformations (FT) for the images from different points in this area (Figure S8 in the Supporting Information). After FT, a repeating set of spots from the Cu lattice were observed. In addition, nonrepeating spots from randomly oriented Cu_2O crystals were found. Inverse FT of the Cu spots did not show imperfect fringes. Therefore, we conclude that the Moiré fringes in Figure 2e and the apparent defect-abundant scattering fringe in Figure 2f were caused by a thin layer (several nanometers in thickness) of polycrystalline Cu_2O formed on the surface of the tip. We suggest that, in the deposition process, the tip was the active growth zone. In this area, the active sites generated many imperfections, which could be oxidized easily into the Cu_2O layer.

In order to understand how the Cu pillars grew, we employed several deposition times. The product that grew initially at 1 h was a layer (0.6−0.8 μm in thickness) of NPs, as shown in the SEM images (Figure S4a,c in the Supporting Information). These NPs were similar to the NPs formed between the nanopillars and the substrate (Figure 1b). In the circled areas in Figure S4a in the Supporting Information, particles manifested the formation of short nanopillars already. As the growth time was increased to 3 h, more nanopillars, 1−2 μm long and 150 ± 25 nm wide, were formed (Figure S4b,d in the Supporting Information). Even though their overall morphology was closely related to those shown in Figure 1, the density and length-to-width aspect ratios were obviously lower than the ones grown at 7 h. On

Scheme 1. Proposed Growth Mechanism of Pagoda-Topped Tetragonal Cu Nanopillars on an Au/Glass Electrode[a]

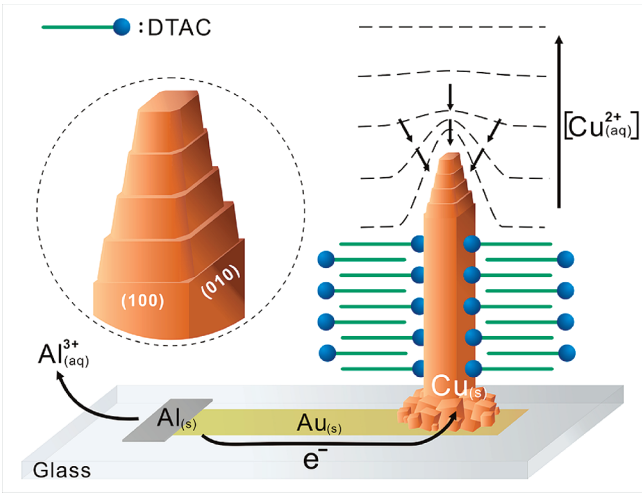

[a] For clarity, only two side faces of the nanopillar are shown to be covered by DTAC.

the basis of the observations, we propose a reaction pathway in Scheme 1 to account for the nanopillar growth. We attribute the formation of this unusual structure to the following reasons. First of all, the over all reduction of Cu^{2+}(aq) by Al(s) to form Cu(s) is thermodynamically favored, as suggested by the reaction $3Cu^{2+}(aq) + 2Al(s) \rightarrow 3Cu(s) + 2Al^{3+}(aq)$, $E_0 = 2.00$ V (20). For this reason, the reaction appears to be fast at the initial growth stage. In this study, a layer of cubelike Cu NPs grew on the substrate after 1 h (Figure S3 in the Supporting Information) (21−26). Apparently, Cu^{2+}(aq) ions near the electrode surface were reduced rapidly to deposit the NPs and served as the seeds for further nanopillar growth. The second important reason is that, in electrochemical deposition systems, diffusion-limited conditions are essential for anisotropic growth (27). In this study, as Cu^{2+}(aq) ions were reduced into Cu(s), a concentration gradient formed near the electrode surface. This diffusion layer would favor anisotropic growth of the crystals. The presence of an adequate amount of DTAC is another important cause. The surfactant molecules probably acted as a capping agent assisting in the shape control of the crystals. It is likely that DTAC self-assembled into a bilayer structure and coadsorbed selectively on Cu{100} crystal planes to confine the branching growth (1, 18, 19). In the absence or deficiency of DTAC, the product grew into a pine-tree-like morphology (Figures S5 and S6a in the Supporting Information). This was also observed for the product grown at an extended deposition time (Figure S5 in the Supporting Information). All stems and branches of the treelike configuration also displayed a tetragonal structure analogous to the nanopillars. Clearly, capping of DTAC molecules on Cu{100} stabilized the facets and minimized extrusion of the branches from the stems. On the other hand, the nanopillar tip with the step-edge structure was less capped. Because the tip was at the bottom of the diffusion layer, more active growth sites were exposed. This allowed more Cu^{2+}(aq) to reduce to Cu(s) for nanopillar elongation

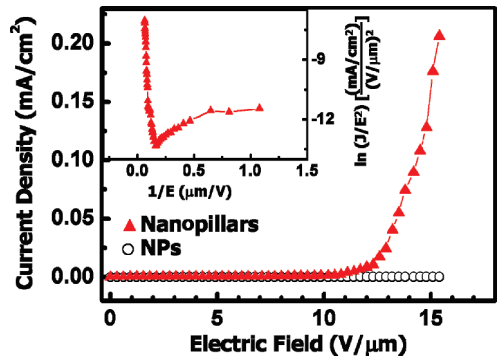

FIGURE 3. Emission current density as a function of the applied electric field on Cu nanopillars and NPs (inset: corresponding FN plots).

(28). An adequate amount of DTAC would passivate the near-perfect {100} side facets for further transverse growth. However, when excess DTAC was added, large clusters were produced (Figure S6b in the Supporting Information). Obviously, too much DTAC suppressed the anisotropic crystal growth condition because the direct galvanic displacement reaction was carried out at near-equilibrium conditions. This caused isotropic growth of a polyhedron or sphere-shaped crystals (27). Another interesting question is, why is the tip of the Cu nanopillar pagoda-shaped instead of other appearances? After the nanocrystal grown initially reconstructs and reshapes so that {100} planes are capped and stabilized by DTAC, Cu ions are more likely to be reduced on the less capped {111} or {110} planes. This would lengthen the nanocrystal into a nanopillar. Because the deposition rates of Cu atoms on different crystal facets at the tip are different, especially in the presence of an adequate amount of DTAC, a pagoda-shaped tip is formed to reveal their differences in stabilization. According to a common crystal growth model, the as-deposited Cu atoms would adhere to more active sites at steps and edges. If Cu atoms deposit on all steps and edges on a pagoda-shaped tip at the same rate, the physical appearance of the tip would be preserved as it elongates.

Because of their novel morphology, field-emission (FE) properties of the pagoda-topped nanopillar arrays were investigated. Because the presence of the Cu_2O layer could influence the emission character, we kept our samples under a nitrogen atmosphere to minimize their exposure to oxygen. For a typical sample, Figure 3 shows that the current density (J) of the emitted electrons increases dramatically over an electric field (E) threshold, the turn-on E, E_0. At E_0 of 12.4 V μm^{-1}, the J value is observed to be 10 μA cm^{-2}. The inset shows a plot of $\ln(J/E^2)$ versus $1/E$. For $1/E$ between 0.06 and 0.15 μm V^{-1}, a nearly straight line is observed. This indicates that the FE character follows that of the model described by the Fowler−Nordheim (FN) equation $J = A(\beta^2E^2/\Phi)\exp(-B\Phi^{3/2}/\beta E)$ (29). In the equation, in addition to J and E mentioned above, Φ is the work function of Cu (4.47 eV) and A and B are constants, 1.56×10^{-10} (A V^{-2} eV^{-1}) and 6.83×10^3 (V $eV^{-3/2}$ μm^{-1}), respectively (14). β is the field enhancement factor, a general parameter describing the emitter performance. β depends on the geometry and morphology of the nanostructure, the

crystal structure of the material, and the density of the emitting points. Here, β is calculated to be 713 (14, 29) by assuming that the thin oxide layer affects the emission little. In contrast, a layer of cubelike Cu NPs deposited at 1 h does not show significant J within the field applied. With their high aspect ratios and unique pagoda-shaped tips, it is not a surprise that the nanopillars can extrude electrons much more efficiently than the NPs. In addition, β of the Cu nanopillars is superior to those of the other 1D Cu nanostructures reported previously, such as the NWs grown by hard-template-assisted and CVD processes, 245 and 443, respectively (13, 15).

In conclusion, we have achieved a simple process to grow arrays of pagoda-topped tetragonal Cu nanopillars with {100} side faces. The growth time and DTAC concentration affect the product morphology significantly. FE measurement shows that the Cu nanopillars can emit electrons under relatively low electric field strength. The pagoda-shaped tip is the growth zone containing many active growth sites. Thus, the tip may serve as an effective sample for understanding crystal growth processes in future studies. Also, the seeding layer plays an important role. We suggest that, by applying uniformly sized and shaped nanocrystals, such as nanocubes, as the seeding layer, controlled growth of Cu nanopillars could be achieved (30). We anticipate that this novel material could be employed for interesting nanodevice applications in the future.

EXPERIMENTAL SECTION

Preparation of Au/Glass Substrate. A glass substrate ($5 \times 10 \times 1$ mm^3) was ultrasonically cleaned in alcohol and acetone for 10 min sequentially. The substrate was masked with Scotch tape to leave an exposed rectangular surface (1.5×4 mm^2). Then, a layer of Au with a thickness of 5 nm was deposited onto the substrate by direct-current sputtering (2.2 kV, 15 mA, and 120 s). Finally, the tape mask was removed to offer the Au electrode. A piece of Al metal sheet ($1 \times 2 \times 0.5$ mm^3) was ultrasonically cleaned in alcohol (5 min) and H_3PO_4(aq) (Riedal-de Haen, 5%, 2 min) and finally rinsed with deionized water. The Al slice was then attached to one side of the Au electrode by silver paste (Toyobo) and dried on a hot plate (353 K, 1 h).

Growth of Cu Nanostructures. The whole glass substrate was immersed into a limpid aqueous solution (4 mL) containing $CuCl_2$ (5 mM, Strem) and DTAC (0.15 mM, Fluka) in a glass vial at 290 K without stirring. The golden electrode turned black rapidly from its edge to the center within 2 min. As the reaction proceeded, it turned to dark red gradually. After a designated period of time (1, 3, and 7 h), the substrate was removed, rinsed by deionized water, dried in a desiccator, and then stored in a nitrogen-filled glovebox before further characterization.

Instruments. The electrodes were characterized by the following instruments: SEM (JEOL JSM-6330F at 15 kV), EDS (Oxford Link Pentafet), TEM (JEOL JEM-2010F at 200 kV and JEOL JEM-4000EX), and XRD (Bruker AXS D8 Advance). Current−voltage properties from FE measurements were carried out using a needle-shaped anode with an effective tip-to-sample distance of 65 μm in a vacuum chamber at 4×10^{-6} torr at room temperature. A positive voltage swept up to 1 kV with a step of 50 V was applied to the anode using a Keithly 2410 power supply.

Acknowledgment. This work is supported by the National Science Council and "Aim for the Top University Plan" of the National Chiao Tung University and the Ministry of Education of Taiwan, Republic of China.

Supporting Information Available: XRD, SEM, TEM, SAED, HRTEM, FT, and inversed FT of TEM. This material is available free of charge via the Internet at http://pubs.acs.org.

REFERENCES AND NOTES

(1) Murphy, C. J.; Sau, T. K.; Gole, A. M.; Orendorff, C. J.; Gao, J.; Gou, L.; Hunyadi, S. E.; Li, T. *J. Phys. Chem. B* **2005**, *109*, 13857.
(2) Nikoobakht, B.; El-Sayed, M. A. *J. Phys. Chem. A* **2003**, *107*, 3372.
(3) Grand, J.; de la Chapelle, M. L.; Bijeon, J. L.; Adam, P. M.; Vial, A.; Royer, P. *Phys. Rev. B* **2005**, *72*, 33407.
(4) Hernandez, J.; Solla-Gullon, J.; Herrero, E.; Aldaz, A.; Feliu, J. M. *J. Phys. Chem. B* **2005**, *109*, 12651.
(5) Langford, R. M.; Wang, T. X.; Thornton, M.; Heidelberg, A.; Sheridan, J. G.; Leahy, W.; Blau, R. *J. Vac. Sci. Technol. B* **2006**, *24*, 2306.
(6) Hsia, C.-H.; Yen, M.-Y.; Lin, C.-C.; Chiu, H.-T.; Lee, C.-Y. *J. Am. Chem. Soc.* **2003**, *125*, 9940.
(7) Yen, M.-Y.; Chiu, C.-W.; Hsia, C.-H.; Chen, F.-R.; Kai, J.-J.; Lee, C.-Y.; Chiu, H.-T. *Adv. Mater.* **2003**, *15*, 235.
(8) Choi, J.; Goring, G.; Sauer, P.; Nielsch, K.; Wehrspohn, R. B.; Gosele, U. *J. Mater. Chem.* **2003**, *13*, 1100.
(9) Liu, J.; Duan, J. L.; Toimil-Molares, M. E.; Karim, S.; Cornelius, T. W.; Dobrev, D.; Yao, H. J.; Sun, Y. M.; Hou, M. D.; Mo, D.; Wang, Z. G.; Neumann, R. *Nanotechnology* **2006**, *17*, 1922.
(10) Li, N.; Li, X.; Yin, X.; Wang, W.; Qiu, S. *Solid State Commun.* **2004**, *132*, 841.
(11) Choi, J.; Sauer, G.; Nielsch, K.; Wehrspohn, R. B.; Gosele, U. *Chem. Mater.* **2003**, *15*, 776.
(12) Dangwal, A.; Pandey, C. S.; Muller, G.; Karim, S.; Cornelius, T. W.; Trautmann, C. *Appl. Phys. Lett.* **2008**, *92*, 3.
(13) Maurer, F.; Dangwal, A.; Lysenkov, D.; Muller, G.; Toimil-Molares, M. E.; Trautmann, C.; Brotz, J.; Fuess, H. *Nucl. Instrum. Methods Phys. Res., Sect. B* **2006**, *245*, 337.
(14) Wang, J.-H.; Yang, T.-H.; Wu, W.-W.; Chen, L.-J.; Chen, C.-H.; Chu, C.-J. *Nanotechnology* **2006**, *17*, 719.
(15) Kim, C.; Gu, W.; Briceno, M.; Robertson, I. M.; Choi, H.; Kim, K. K. *Adv. Mater.* **2008**, *20*, 1859.
(16) Xiong, Y.; Cai, H. B.; Wiley, J.; Wang, J.; Kim, M. J.; Xia, Y. *J. Am. Chem. Soc.* **2007**, *129*, 3665.
(17) Wiley, B. J.; Chen, Y.; McLellan, J. M.; Xiong, Y.; Li, Z. Y.; Ginger, D.; Xia, Y. *Nano Lett.* **2007**, *7*, 1032.
(18) Huang, T.-K.; Cheng, T.-H.; Yen, M.-Y.; Hsiao, W.-H.; Wang, L.-S.; Chen, F.-R.; Kai, J.-J.; Lee, C.-Y.; Chiu, H.-T. *Langmuir* **2007**, *23*, 5722.
(19) Huang, T.-K.; Chen, Y.-C.; Ko, H.-C.; Huang, H.-W.; Wang, C.-H.; Lin, H.-K.; Chen, F.-R.; Kai, J.-J.; Lee, C.-Y.; Chiu, H.-T. *Langmuir* **2008**, *24*, 5647.
(20) Bard, A. J.; Faulkner, L. R. *Electrochemical Methods: Fundamentals and Applications*; John Wiley & Sons: New York, 1980.
(21) Wang, Y.; Chen, P.; Liu, M. *Nanotechnology* **2006**, *17*, 6000.
(22) Im, S. H.; Lee, Y. T.; Wiley, B.; Xia, Y. *Angew. Chem., Int. Ed.* **2005**, *44*, 2154.
(23) Yu, D.; Yam, V. W. W. *J. Am. Chem. Soc.* **2004**, *126*, 13200.
(24) Kundu, S.; Panigrahi, S.; Panigrahi, Basu, S.; Ghosh, S. K.; Pal, A.; Pal, T. *Nanotechnology* **2007**, *18*, 75712.
(25) Wang, C.; Daimon, H.; Lee, Y.; Kim, J.; Sun, S. *J. Am. Chem. Soc.* **2007**, *129*, 6974.
(26) Sun, Y.; Zhang, L.; Zhou, H.; Zhu, Y.; Sutter, E.; Ji, Y.; Rafailovich, M. H.; Sokolov, J. C. *Chem. Mater.* **2007**, *19*, 2065.
(27) Fukami, K.; Nakanishi, S.; Yamasaki, H.; Tada, T.; Sonoda, K.; Kamikawa, N.; Tsuji, N.; Sakaguchi, H.; Nakato, Y. *J. Phys. Chem. C* **2007**, *111*, 1150.
(28) Walter, E. C.; Murray, B. J.; Favier, F.; Kaltenpoth, G.; Grunze, M.; Penner, R. M. *J. Phys. Chem. B* **2002**, *106*, 11407.
(29) Fowler, R. H.; Nordheim, L. W. *Proc. R. Soc. London, Ser. A* **1928**, *119*, 173.
(30) Xia, Y.; Xiong, Y.; Lim, B.; Skrabalak, S. E. *Angew. Chem., Int. Ed.* **2009**, *48*, 60.

AM900264U